H-wave – A Python package for the Hartree-Fock approximation and the random phase approximation

Tatsumi Aoyama[a,*], Kazuyoshi Yoshimi[a], Kota Ido[a], Yuichi Motoyama[a], Taiki Kawamura[b], Takahiro Misawa[a], Takeo Kato[a], Akito Kobayashi[b]

[a]*Institute for Solid State Physics, University of Tokyo, Chiba 277-8581, Japan*
[b]*Department of Physics, Nagoya University, Nagoya 464-8602, Japan*

Abstract

H-wave is an open-source software package for performing the Hartree–Fock approximation (HFA) and random phase approximation (RPA) for a wide range of Hamiltonians of interacting fermionic systems. In HFA calculations, H-wave examines the stability of several symmetry-broken phases, such as anti-ferromagnetic and charge-ordered phases, in the given Hamiltonians at zero and finite temperatures. Furthermore, H-wave calculates the dynamical susceptibilities using RPA to examine the instability toward the symmetry-broken phases. By preparing a simple input file for specifying the Hamiltonians, users can perform HFA and RPA for standard Hamiltonians in condensed matter physics, such as the Hubbard model and its extensions. Additionally, users can use a WANNIER90-like format to specify fermionic Hamiltonians. A WANNIER90 format is implemented in RESPACK to derive *ab initio* Hamiltonians for solids. HFA and RPA for the *ab initio* Hamiltonians can be easily performed using H-wave. In this paper, we first explain the basis of HFA and RPA, and the basic usage of H-wave, including download and installation. Thereafter, the input file formats implemented in H-wave, including the WANNIER90-like format for specifying the interacting fermionic Hamiltonians, are discussed. Finally, we present several examples of H-wave such as zero-temperature HFA calculations for the extended Hubbard model on a square lattice, finite-temperature HFA calculations for the Hubbard model on a cubic lattice, and RPA in the extended Hubbard model on a square lattice.

Keywords: Quantum lattice models; Mean field approximation; Random phase approximation

PROGRAM SUMMARY

1. Introduction

Clarifying how electron correlations in solids induce several symmetry-broken phases has long been a crucial issue in the field of condensed matter physics [1, 2]. Although deriving tight-binding models from *ab initio* calculations is now a standard daily procedure [3–5], solving the obtained effective models by considering the effects of Coulomb interactions remains as a non-trivial problem. To

*Corresponding author.
Email addresses: aoym@issp.u-tokyo.ac.jp (Tatsumi Aoyama), k-yoshimi@issp.u-tokyo.ac.jp (Kazuyoshi Yoshimi)

solve effective models numerically, various numerical algorithms such as the exact diagonalization [6], quantum Monte Carlo [7], and tensor network [8–10] methods have been developed to date [11, 12]. However, these algorithms frequently incur high computational cost because they consume a significant amount of memory or execution time.

Numerical algorithms based on the Hartree–Fock approximation (HFA) have long been used in condensed matter physics [13, 14]. Unrestricted HFA (UHFA), which is a simple and fundamental method for treating electronic states in molecules and solids, is used to examine the stability of ordered phases. For example, the HFA has been used for analyzing the ordered phases in the Hubbard model [15, 16], spin and orbital orderings in $3d$ transition-metal oxides [17], and the spin and charge ordered phases in organic compounds [18]. Similarly, random phase approximation (RPA), which is an algorithm for calculating response functions consistent with the UHFA [13, 19, 20], is used for detecting instability toward ordered phases through the divergence of susceptibility. In comparison with other sophisticated algorithms, the main advantage of the UHFA and the RPA is low numerical cost. Therefore, they are suitable for clarifying general trends in ordered phases in correlated electron systems.

Program codes for UHFA and RPA have been implemented and maintained by researchers for specific lattice models. To our knowledge, there are no widely used packages for UHFA and RPA, except for a supplementary RPA package included in triqs [21, 22] and the supplementary real-space UHF package included in mVMC [23]. Recently, HF and RPA analyses combined with first-principles calculations have become popular in treating real materials. When handling such complex models derived from the first-principles calculations, it will take much time to modify existing packages or to newly implement programs. For an easy application of the UHFA and RPA to such complex models, the development of a software package that treats various effective models of solids in a simple format is desirable. Recently, H-wave was released as an open-source Python package with a simple and flexible user interface [24]. Using H-wave, users can perform calculations by applying UHFA and RPA to widely studied quantum lattice models by preparing only one input file with less than ten lines. H-wave can treat the Wannier90-like format and has interfaces for smooth connection with mVMC [23] and

$\mathcal{H}\Phi$ [25], which are program packages for more accurate calculation taking into account electron correlations.

In this paper, we introduce H-wave version 1.0.0. The remainder of this paper is organized as follows. Models that can be treated using H-wave are explained in Sec. 2.1. The basis of the UHFA and RPA is discussed in Secs. 2.2 and 2.3, respectively. In Sec. 3, the basic usage of H-wave, for example, downloading, installing, and running operations, is explained. The formats of the input files, including the Wannier90-like format for specifying the Hamiltonians, are elaborated. Three applications of H-wave are demonstrated in Sec. 4, such as the ground-state UHFA calculations of the extended Hubbard model on a square lattice, finite-temperature UHFA calculations of the Hubbard model on a cubic lattice, and RPA calculations of the extended Hubbard model on a square lattice. Section 5 presents a summary of the study.

2. Model and Algorithm

2.1. Model

In H-wave, the following extended Hubbard model can be treated:

$$\mathcal{H} = \mathcal{H}_0 + \mathcal{H}_{\text{int}}, \tag{1}$$

$$\mathcal{H}_0 = \sum_{\langle i\alpha; j\beta \rangle} \left(t_{ij}^{\alpha\beta} c_{i\alpha}^\dagger c_{j\beta} + \text{H.c.} \right), \tag{2}$$

$$\mathcal{H}_{\text{Int}} = \sum_{i,j,k,l} \sum_{\alpha,\alpha',\beta,\beta'} \mathcal{I}_{ijkl}^{\alpha\alpha'\beta\beta'} c_{i\alpha}^\dagger c_{j\alpha'} c_{k\beta}^\dagger c_{l\beta'}, \tag{3}$$

where i, j, k, and l $(\in 0, \cdots, N_{\text{site}} - 1)$ denote the lattice points with N_{site} being the number of lattice sites, and α, α', β, and β' specify the general orbitals including the orbitals and spins in a unit cell. $c_{i\alpha}^\dagger$ $(c_{i\alpha})$ is the creation (annihilation) operator for an electron with a general orbital α at the ith site. $\langle i\alpha; j\beta \rangle$ and $t_{ij}^{\alpha\beta}$ represent the bond pair and the hopping integral between sites (i, α) and (j, β), respectively. $\mathcal{H}_{\text{Int}}$ is a general two-body Hamiltonian and the two-body interaction satisfies $\mathcal{I}_{ijkl}^{\alpha\alpha'\beta\beta'} = \left[\mathcal{I}_{lkji}^{\beta'\beta\alpha'\alpha} \right]^*$ for satisfying the Hermiticity.

2.2. Unrestricted Hartree–Fock approximation

In the unrestricted Hartree-Fock approximation (UHFA), we can decouple the general two-body in-

teractions as

$$c_I^\dagger c_J c_K^\dagger c_L = -c_I^\dagger c_K^\dagger c_J c_L + c_I^\dagger c_L \delta_{J,K}$$

$$\sim -\langle c_I^\dagger c_L \rangle c_K^\dagger c_J - c_I^\dagger c_L \langle c_K^\dagger c_J \rangle + \langle c_I^\dagger c_J \rangle c_K^\dagger c_L$$

$$+ c_I^\dagger c_J \langle c_K^\dagger c_L \rangle + \left(\langle c_I^\dagger c_L \rangle \langle c_K^\dagger c_J \rangle - \langle c_I^\dagger c_J \rangle \langle c_K^\dagger c_L \rangle \right)$$

$$+ c_I^\dagger c_L \delta_{J,K}, \quad (4)$$

where we adopt $I \equiv (i, \alpha)$, $J \equiv (j, \alpha')$, $K \equiv (k, \beta')$, and $L \equiv (l, \beta)$ as notations for brevity, and the Kronecker's delta is denoted as $\delta_{J,K}$. Using the UHFA, the Hamiltonian is generally denoted as

$$\mathcal{H}_{\mathrm{UHFA}} = \sum_{I,J} c_I^\dagger H_{IJ} c_J = \boldsymbol{c}^\dagger \boldsymbol{H} \boldsymbol{c}, \quad (5)$$

where $\boldsymbol{H}$ denotes a matrix with elements represented as H_{IJ}, and $\boldsymbol{c}$ ($\boldsymbol{c}^\dagger$) represents a column (row) vector with elements denoted as c_I ($c_I^\dagger$). Since $\boldsymbol{H}$ is an Hermite matrix, the Hamiltonian can be diagonalized by the unitary matrix $\boldsymbol{U}$ as

$$\boldsymbol{H}_{\mathrm{UHFA}} = \boldsymbol{U} \boldsymbol{\Lambda} \boldsymbol{U}^\dagger, \quad \boldsymbol{\Lambda} = \mathrm{diag}(\lambda_0, \lambda_1, \dots) \quad (6)$$

where λ_n represents the nth eigenvalue of $\boldsymbol{H}$. By defining $\boldsymbol{d} = \boldsymbol{U}^\dagger \boldsymbol{c}$, $\mathcal{H}_{\mathrm{UHFA}}$ can be rewritten as

$$\mathcal{H}_{\mathrm{UHFA}} = \boldsymbol{d}^\dagger \boldsymbol{\Lambda} \boldsymbol{d} = \sum_n \lambda_n d_n^\dagger d_n. \quad (7)$$

Thus, the free energy from the UHFA can be expressed as

$$F = \mu N_e - \frac{1}{\beta} \sum_n \ln \left[1 + \exp(-\beta(\lambda_n - \mu)) \right]$$

$$+ \sum_{I,J,K,L} \mathcal{I}_{IJKL} \left(\langle c_I^\dagger c_L \rangle \langle c_K^\dagger c_J \rangle - \langle c_I^\dagger c_J \rangle \langle c_K^\dagger c_L \rangle \right), \quad (8)$$

where β denotes the inverse temperature, N_e is the total number of particles, and μ represents the chemical potential.

In the UHFA calculations, we start from the initial one-body Green's functions, which are then updated as

$$\langle c_I^\dagger c_J \rangle = \sum_n U_{In}^* U_{Jn} \langle d_n^\dagger d_n \rangle = \sum_n \frac{U_{In}^* U_{Jn}}{1 + e^{\beta(\lambda_n - \mu)}}. \quad (9)$$

In the canonical calculation in which the number of particles is fixed to N_e, μ is determined to satisfy

the relation $N_e = \sum_I \langle c_I^\dagger c_I \rangle$ at every step. In H-wave, the simple-mixing algorithm is employed to update the one-body Green's functions, which are defined as

$$\langle c_I^\dagger c_J \rangle^{(n+1)} \leftarrow (1 - \alpha_{\mathrm{mix}}) \langle c_I^\dagger c_J \rangle^{(n)} + \alpha_{\mathrm{mix}} \langle c_I^\dagger c_J \rangle^{(n+1)}, \quad (10)$$

where $\langle c_I^\dagger c_J \rangle^{(n)}$ represents the Green's functions at the nth step and α_{mix} denotes a parameter between 0 and 1. The iterations are repeated until the convergence condition is satisfied in which the residue R becomes smaller than a given criterion ε, such that

$$R = \frac{1}{2 N_{\mathrm{site}}^2} \sqrt{ \sum_{IJ} \left| \langle c_I^\dagger c_J \rangle^{(n+1)} - \langle c_I^\dagger c_J \rangle^{(n)} \right|^2 } < \varepsilon. \quad (11)$$

The calculation is unsuccessful or fails if the convergence condition is not met within a specified number of iterations. In Fig. 1, a schematic flow of the calculation of the UHFA calculation is shown for convenience.
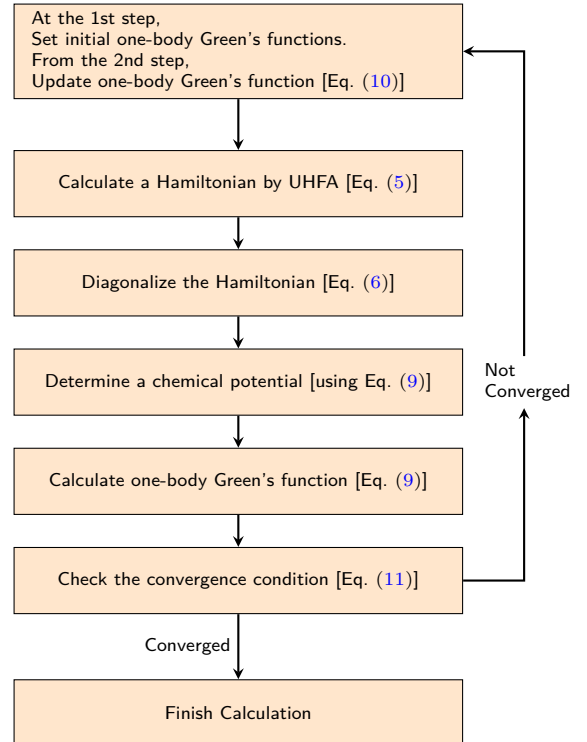

Figure 1: Schematic flow of the UHFA calculation.

2.2.1. Hartree–Fock approximation in the momentum space

When a two-body Hamiltonian satisfies the translational symmetry, we can efficiently perform the HFA calculation in the momentum space. In the following, the translational-invariant two-body Hamiltonian below is considered instead of Eq. (3)

$$\mathcal{H}_{\mathrm{Int}} \equiv \sum_{ij} \sum_{\alpha,\alpha',\beta,\beta'} W_{ij}^{\alpha\alpha'\beta\beta'} c_{i\alpha}^{\dagger} c_{i\alpha'} c_{j\beta}^{\dagger} c_{j\beta'}, \tag{12}$$

where a two-body interactions satisfies $W_{ij}^{\alpha\alpha'\beta\beta'} = \left[W_{ji}^{\beta'\beta\alpha'\alpha} \right]^*$ for the Hermiticity. The Fourier transformations of the operator are defined as

$$c_{\boldsymbol{r}_i\alpha} = \frac{1}{\sqrt{N_{\mathrm{site}}}} \sum_{\boldsymbol{k}} e^{i\boldsymbol{k}\cdot\boldsymbol{r}_i} c_{\boldsymbol{k}\alpha}, \tag{13}$$

$$c_{\boldsymbol{r}_i\alpha}^{\dagger} = \frac{1}{\sqrt{N_{\mathrm{site}}}} \sum_{\boldsymbol{k}} e^{-i\boldsymbol{k}\cdot\boldsymbol{r}_i} c_{\boldsymbol{k}\alpha}^{\dagger}, \tag{14}$$

where N_{site} denotes the number of the sites and $\boldsymbol{r}_i$ is a position vector at the ith site. The one-body Hamiltonian in the real space is rewritten as

$$h_0 = \sum_{\boldsymbol{k},\alpha,\beta} c_{\boldsymbol{k}\alpha}^{\dagger} h_{\alpha\beta}(\boldsymbol{k}) c_{\boldsymbol{k}\beta}. \tag{15}$$

Since the system has a translational symmetry, the coefficients depend only on the translation vectors, $\boldsymbol{r}_{ij} = \boldsymbol{r}_j - \boldsymbol{r}_i$ and $h_{\alpha\beta}(\boldsymbol{k}) = \sum_j \tilde{t}_{0j}^{\alpha\beta} e^{-i\boldsymbol{k}\cdot\boldsymbol{r}_{0j}}$, where $\tilde{t}_{0j}^{\alpha\beta}$ includes $t_{0j}^{\alpha\beta}$ and the decoupled two-body interaction terms. As the Hamiltonian is diagonal with respect to the wave number $\boldsymbol{k}$, the eigenvalue and eigenvector calculations are simplified from the diagonalization of the matrix of the size $N_{\mathrm{site}}N_{\mathrm{orbit}} \times N_{\mathrm{site}}N_{\mathrm{orbit}}$ to that of N_{site} matrices of the size $N_{\mathrm{orbit}} \times N_{\mathrm{orbit}}$, where N_{orbit} denotes the number of orbitals, including the spin degrees of freedom. Thus, the calculation costs are reduced.

2.3. Random Phase Approximation

The random phase approximation (RPA) is used for calculating the response functions, such as charge/spin susceptibility. By examining the temperature dependence of the charge/spin susceptibility, the instability of charge/spin ordered phases can be detected. In H-wave, RPA can be implemented in momentum space and users can obtain the dynamical susceptibility $\chi(\boldsymbol{q}, i\nu_n)$, where ν_n represents the bosonic Matsubara frequency, $\nu_n = $

$2n\pi k_B T$ ($n = -N_\omega/2, \cdots, N_\omega/2 - 1$) with the even cutoff integer N_ω. Here, T is the temperature and k_B is the Boltzmann constant, and for simplicity, we set $k_B = 1$ in the following. We note that it is necessary to perform the analytical continuation to obtaining the real-frequency dynamical susceptibility $\chi(\boldsymbol{q}, \omega)$, which can be measured by experiments. In this section, we briefly introduce the method for calculating the dynamical susceptibility using the RPA.

By applying Fourier transformation to the two-body Hamiltonian $\mathcal{H}_{\mathrm{Int}}$ defined in Eq. (12), the Hamiltonian can be rewritten as

$$\mathcal{H}_{\mathrm{Int}} = \frac{1}{2N_{\mathrm{site}}} \sum_{\boldsymbol{k},\boldsymbol{k}',\boldsymbol{q}} \sum_{\alpha,\alpha',\beta,\beta'} W_{\boldsymbol{q}}^{\alpha\alpha'\beta\beta'}$$
$$\times c_{\boldsymbol{k}+\boldsymbol{q},\alpha}^{\dagger} c_{\boldsymbol{k},\alpha'} c_{\boldsymbol{k}'-\boldsymbol{q},\beta}^{\dagger} c_{\boldsymbol{k}',\beta'}. \tag{16}$$

In the RPA, the scattering processes by the interaction are considered on the basis of eigenvectors of the non-interacting Hamiltonian $\mathcal{H}_0$. On this basis, the two-body interaction operator can be approximated as

$$c_{\boldsymbol{k}+\boldsymbol{q},\alpha}^{\dagger} c_{\boldsymbol{k},\alpha'} c_{\boldsymbol{k}'-\boldsymbol{q},\beta}^{\dagger} c_{\boldsymbol{k}',\beta'}$$
$$\sim \sum_{\gamma,\gamma'} u_{\alpha\gamma,\boldsymbol{k}+\boldsymbol{q}}^* u_{\alpha'\gamma,\boldsymbol{k}} u_{\beta\gamma',\boldsymbol{k}'-\boldsymbol{q}}^* u_{\beta'\gamma',\boldsymbol{k}'}$$
$$\times d_{\boldsymbol{k}+\boldsymbol{q},\gamma}^{\dagger} d_{\boldsymbol{k},\gamma} d_{\boldsymbol{k}'-\boldsymbol{q},\gamma'}^{\dagger} d_{\boldsymbol{k}',\gamma'}, \tag{17}$$

where $c_{\boldsymbol{k},\alpha} = \sum_\gamma u_{\alpha\gamma,\boldsymbol{k}} d_{\boldsymbol{k},\gamma}$, and $d_{\boldsymbol{k},\gamma}$ denotes the annihilation operator that diagonalizes $\mathcal{H}_0$. (γ denotes the eigenvalue index.) Then, the irreducible one-body Green's function can be expressed as

$$G_\gamma^{(0)\alpha\beta}(\boldsymbol{k}, i\omega_n) = \frac{u^{\alpha\gamma}(\boldsymbol{k}) u^{*\beta\gamma}(\boldsymbol{k})}{i\omega_n - \xi^\gamma(\boldsymbol{k}) + \mu}, \tag{18}$$

where ω_n represents the fermionic Matsubara frequency $\omega_n = (2n+1)\pi T$. Generally, the irreducible susceptibility in non-interacting systems can be expressed as

$$\chi^{(0)\alpha\alpha',\beta'\beta}(\boldsymbol{q}, i\nu_n) =$$
$$-\frac{T}{N_{\mathrm{site}}} \sum_{\gamma=1}^{N_{\mathrm{orbit}}} \sum_{\boldsymbol{k},m} G_\gamma^{(0)\alpha\beta}(\boldsymbol{k}+\boldsymbol{q}, i\omega_m + i\nu_n)$$
$$\times G_\gamma^{(0)\beta'\alpha'}(\boldsymbol{k}, i\omega_m). \tag{19}$$

By using the irreducible susceptibility, the dynamical susceptibility from the RPA, $\chi^{\alpha\alpha',\beta'\beta}(\boldsymbol{q}, i\nu_n)$,

can be obtained as

$$
\chi^{\alpha\alpha',\beta'\beta}(q) = \chi^{(0)\alpha\alpha',\beta'\beta}(q)
$$
$$
- \sum_{\alpha'_1\beta'_1} \chi^{(0)\alpha\alpha',\beta'_1\beta_1}(q)\, W_{\boldsymbol{q}}^{\alpha_1\alpha'_1\beta'_1\beta_1}\, \chi^{\alpha_1\alpha'_1,\beta'\beta}(q),
$$
$$(20)$$

where we define $q \equiv (\boldsymbol{q}, i\nu_n)$ for simplicity. Here, the index α includes the orbital and spin degrees of freedom. By combining indices into one index, for example, $a = \alpha \times \alpha'$, Eq. (20) can be rewritten in a matrix form as

$$
\boldsymbol{\chi}(q) = \boldsymbol{\chi}^{(0)}(q) - \boldsymbol{\chi}^{(0)}(q)\boldsymbol{W}(q)\boldsymbol{\chi}(q)
$$
$$
= \left[\boldsymbol{I} + \boldsymbol{\chi}^{(0)}(q)\boldsymbol{W}(q)\right]^{-1} \boldsymbol{\chi}^{(0)}(q), \qquad (21)
$$

where I denotes the identity matrix. Here, for describing the equation in matrix notation, we define the two-body interaction $[\boldsymbol{W}(q)]^{ab} \equiv W_{\boldsymbol{q}}^{ba}$. The dimensions of the susceptibilities $\chi^{(0)\alpha\alpha'\beta'\beta}(\boldsymbol{q}, i\nu_n)$ and $\chi^{\alpha\alpha',\beta'\beta}(\boldsymbol{q}, i\nu_n)$ are given by $N_{\mathrm{orbit}}^4 N_{\mathrm{site}} N_\omega$.

The size of the multidimensional array of susceptibilities can be reduced by separating orbitals and spins. When the spin-orbital coupling does not exist and $\mathcal{H}$ does not include terms that mix spin and orbital, the orbital and spin Hilbert spaces become independent. In this case, the two-body interaction can be rewritten as

$$
W_{\boldsymbol{q}}^{\alpha_{\sigma\sigma'}\beta_{\sigma_1\sigma'_1}} c_{\boldsymbol{k}+\boldsymbol{q},\alpha\sigma}^\dagger c_{\boldsymbol{k},\alpha\sigma'} c_{\boldsymbol{k}'-\boldsymbol{q},\beta\sigma_1}^\dagger c_{\boldsymbol{k}',\beta\sigma'_1}, \quad (22)
$$

where $\alpha_{\sigma\sigma'} \equiv \alpha\sigma\alpha\sigma'$ and $\beta_{\sigma_1\sigma'_1} \equiv \beta\sigma_1\beta\sigma'_1$. Since the scattering processes occur only on the same diagonalized general orbitals, the irreducible susceptibility can be expressed as

$$
\chi_{\sigma\sigma'\sigma'_1\sigma_1}^{(0)\alpha,\beta}(\boldsymbol{q}, i\nu_n) =
$$
$$
-\frac{T}{N_{\mathrm{site}}} \sum_{\gamma=1}^{N_{\mathrm{orb}}} \sum_{\boldsymbol{k},m} G_{\sigma\sigma'_1,\gamma}^{(0)\alpha\beta}(\boldsymbol{k}+\boldsymbol{q}, i\omega_m + i\nu_n)
$$
$$
\times G_{\sigma_1\sigma',\gamma}^{(0)\beta\alpha}(\boldsymbol{k}, i\omega_m). \quad (23)
$$

Here, the array size can be reduced to $N_{\mathrm{orb}}^2 N_{\mathrm{spin}}^4 N_{\mathrm{site}} N_\omega$ where N_{orb} and N_{spin} denote the number of the orbital and spin degrees of freedom, respectively. Then, the susceptibility can

be obtained as

$$
\chi_{\sigma\sigma'\sigma'_1\sigma_1}^{\alpha,\beta}(q) = \chi_{\sigma\sigma'\sigma'_1\sigma_1}^{(0)\alpha,\beta}(q)
$$
$$
- \sum_{\alpha_2\alpha_3} \sum_{\sigma_2,\sigma'_2} \sum_{\sigma_3,\sigma'_3} \chi_{\sigma\sigma'\sigma'_2\sigma_2}^{(0)\alpha,\alpha_2}(q)
$$
$$
\times W_{\boldsymbol{q}}^{\alpha_3\sigma_3\sigma'_3\alpha_2\sigma'_2\sigma_2} \chi_{\sigma_3\sigma'_3,\sigma'_1\sigma_1}^{\alpha_3,\beta}(q). \quad (24)
$$

Like as deriving Eq. (20), if $\alpha_{\sigma\sigma'}$ is represented as a single index, it can be inserted into a matrix form, and for generalized orbitals it can be denoted as

$$
\boldsymbol{\chi}(q) = \boldsymbol{\chi}^{(0)}(q) - \boldsymbol{\chi}^{(0)}(q)\boldsymbol{W}(q)\boldsymbol{\chi}(q)
$$
$$
= \left[\boldsymbol{I} + \boldsymbol{\chi}^{(0)}(q)\boldsymbol{W}(q)\right]^{-1} \boldsymbol{\chi}^{(0)}(q). \quad (25)
$$

In the above formula, it is necessary to store $G_{\sigma_1\sigma',\gamma}^{(0)\beta\alpha}(\boldsymbol{k}, i\omega_n)$ and align the indices of γ for $G_{\sigma_1\sigma',\gamma}^{(0)\beta\alpha}(\boldsymbol{k}, i\omega_n)$ before the summation of γ. However, these procedures increase the numerical cost. To reduce the numerical cost, in previous studies [26–33] the one-body Green's function is simply calculated as $G_{\sigma\sigma'}^{(0)\alpha\beta}(\boldsymbol{k}, i\omega_n) = \sum_{\gamma=1}^{N_{\mathrm{orb}}} G_{\sigma\sigma',\gamma}^{(0)\alpha\beta}(\boldsymbol{k}, i\omega_n)$. Therefore, the irreducible susceptibility is calculated as

$$
\chi_{\sigma\sigma'\sigma_1\sigma'_1}^{(0)\alpha,\beta}(\boldsymbol{q}, i\nu_n) =
$$
$$
-\frac{T}{N_{\mathrm{site}}} \sum_{\boldsymbol{k},m} G_{\sigma\sigma'_1}^{(0)\alpha\beta}(\boldsymbol{k}+\boldsymbol{q}, i\nu_n + i\omega_m)
$$
$$
\times G_{\sigma_1\sigma'}^{(0)\beta\alpha}(\boldsymbol{k}, i\omega_m). \quad (26)
$$

Since additional terms, $G_{\sigma\sigma'_1,\gamma}^{(0)\alpha\beta}(\boldsymbol{k} + \boldsymbol{q}, i\nu_m + i\omega_n) G_{\sigma_1\sigma',\gamma'}^{(0)\beta\alpha}(\boldsymbol{k}, i\omega_n)$ for $\gamma \neq \gamma'$ are included, it can lead to quantitatively different results. Although this treatment is an *approximation* of the original RPA equations defined in Eq. (25), we adopted this approach. We note that when this approximation is applied to orbitals that are clearly independent, a qualitative difference appears because it takes into account the hybridization of orbitals that do not originally exist. After performing the block diagonalization, it is expected to closely agree with the exact RPA when only specific modes are essential, such as near the transition point. However, quantitative deviations will occur away from the transition point. In the next version of the software, a mode for the correct handling of the Green's functions and susceptibilities to examine the accuracy of the approximation method will be implemented.

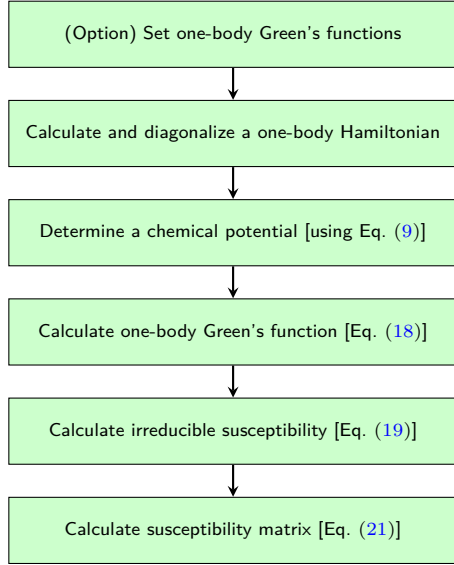Finally, for convenience, a schematic flow of the RPA calculation is presented in Fig. 2.

Figure 2: Schematic flow of the RPA calculation.

3. Usage

3.1. Installing H-wave

H-wave is implemented in Python3 and requires several external libraries, such as NumPy [34, 35], SciPy [36, 37], tomli [38], and requests [39]. Since H-wave is registered to the Python Package Index (PyPI) repository [40], users can install H-wave using the command-line tool `pip` as

```
$ python3 -m pip install h-wave
```

Additionally, the required libraries are installed.

The source code for H-wave is available in the GitHub repository [41]. The users can download the zipped file from the release page, or clone the repository to obtain the latest version. After unpacking the zipped source files and changing the current directory to the top of the source tree, users can install H-wave by executing the following command.

```
$ python3 -m pip install .
```

Subsequently, H-wave and the required libraries are installed, and the executable file `hwave` is placed in the specified installation path. Further details are provided in the installation section of the manual [42].
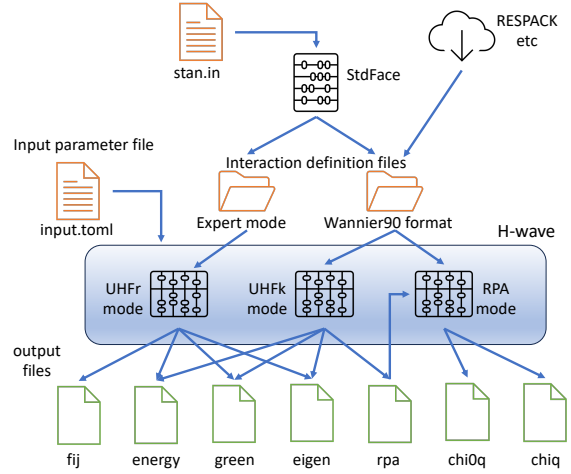

Figure 3: Schematic flow of calculations. First, the users prepare an input parameter file (`input.toml`) and a set of interaction definition files. The interaction definition files can be generated by StdFace from a simple definition file (`stan.in`), or the output of other software such as RESPACK[43] can be used. Then, H-wave is run in a chosen mode. The results are provided as output in the files according to the input parameters.

3.2. Using H-wave

To use H-wave, a TOML-format file (e.g., `input.toml`) and input files that specify the parameters in the Hamiltonians have to be prepared. Figure 3 shows the schematic flow of the calculations. In the TOML file, the calculation parameters and the names of the input files for the Hamiltonian are specified. For standard models such as the Hubbard model on a square lattice, users can use the StdFace library [44] to generate the input files that specify the Hamiltonians. Users can run H-wave by executing the following command.

```
$ hwave input.toml
```

When the calculations are complete, the results are provided as outputs to the files, which are specified by `input.toml`.

3.2.1. Input parameter file

The input parameter file is written in the TOML-format [45] text file. In the TOML format, the value of a parameter is specified in the form `parameter = value`, where the value can be a string, number, Boolean value, array, or table (associative array). A set of parameters can be classified into a TOML table structure and labeled by a name within a square bracket, which we call a *section* hereafter. An example of `input.toml` is presented below:

```
[log]
  print_level = 1
  print_step = 10
[mode]
  mode = "UHFk"
[mode.param]
  2Sz = 0
  Ncond = 16
  IterationMax = 1000
  EPS = 12
  Mix = 0.5
  RndSeed = 123456789
  ene_cutoff = 1.0e+2
  T = 0.0
  CellShape = [ 4, 4, 1 ]
  SubShape = [ 2, 2, 1 ]
[file]
[file.input]
  path_to_input = ""
[file.input.interaction]
  path_to_input = "./"
  Geometry = "geom.dat"
  Transfer = "transfer.dat"
  CoulombIntra = "coulombintra.dat"
[file.output]
  path_to_output = "output"
  energy = "energy.dat"
  eigen = "eigen"
  green = "green"
```

Important sections used in `input.toml`, such as [mode], [mode.param], [log], [file.input], and [file.output] are discussed in this paper. Further details have been provided in the manual of H-wave [42].

[mode]— In the `mode` section, the calculation mode is specified as

```
[mode]
mode = "UHFk"
```

As aforementioned, H-wave implements three methods, UHFA in real space (`mode="UHFr"`), UHFA in wave-number space (`mode="UHFk"`), and RPA (`mode="RPA"`). During the UHFA calculations, decision to include the Fock term can be specified using `flag_fock`. In the wave-number space UHFA and RPA calculations, `enable_spin_orbital` can be used to allow the hopping integrals that break the total S_z conservation. If the total S_z is conserved, the calculation cost of RPA can be significantly reduced. See Sec. 4.2.2 of the H-wave manual
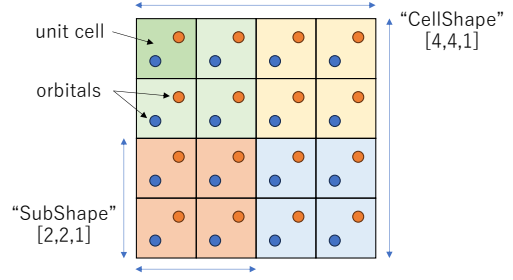

Figure 4: The definitions of the overall lattice (CellShape) and the sublattice structure (SubShape) are depicted with examples.

for the index rule of the orbitals and spins when the `enable_spin_orbital` is set to true.

[mode.param]—In the `mode.param` section, the parameters concerning the calculation conditions can be specified. The lattice size (the number of sites) is specified using `CellShape` (`Nsite`). For the wave-number space UHFA and RPA calculations, a sub-lattice structure can be introduced using `SubShape`, as depicted in Fig. 4. The temperature is denoted by `T`. The number of electrons is specified using `Ncond` or by `filling` ratio to the total number of states. In the UHFA calculations, the total spin can be specified using `2Sz`, or it can be left free.

The mean-field approximation is iteratively solved using the convergence criterion given by the `EPS` parameter. For the RPA calculations, the number of Matsubara frequencies is specified using `Nmat`. For sufficiently large Matsubara frequency, the Green's function behaves like $1/i\omega_n$. The high-energy tail of the Green's functions along the Matsubara frequencies can be improved by subtracting $a/i\omega_n$, which can be treated analytically. The coefficient of the subtraction term a can be specified through `coeff_tail`. Basically, the default value $a = 1$ works well, but for more precise work, it may be better to select a as $i\omega_{n_{\max}} G(i\omega_{n_{\max}})$.

[log]— In the `log` section, the conditions of calculation logs can be specified. `print_level` is used to specify the verbosity of the log outputs. In the UHFA calculations, the interval between the residue outputs during the iterations can be set using `print_step`. When specified, the residues are written to the files given by `print_check`.

[file.input]— In the `file.input` section, the input files can be specified. The files that define the Hamiltonians are specified in a separate subsection [file.input.interaction], as described

7

in Sec. 3.2.2. In this section, the file name of the initial Green's function can be specified using `initial` parameter. In the RPA calculations, the interaction term approximated using the UHFA can be considered for the initial configuration. The coefficient of the modified hopping term $\widetilde{\mathcal{H}_0} = \sum \widetilde{t_{ij}^{\alpha\beta}} c_{i\alpha}^\dagger c_{j\beta} + H.c.$, where

$$\widetilde{t_{ij}^{\alpha\beta}} = t_{ij}^{\alpha\beta} + \sum_{k,\gamma,\gamma'} W_{ik}^{\gamma\gamma',\alpha\beta} \langle c_{k\gamma'}^\dagger c_{k\gamma} \rangle \delta_{ij}, \quad (27)$$

can be read from a file specified by `trans_mod`. The input file can be generated through a wave-number space UHFA calculation using the `rpa` output option. An option for using the irreducible susceptibility $\chi^{(0)}(\boldsymbol{q})$ specified by `chi0q`, which is obtained from the former calculation, is available for the calculation of the susceptibility matrix.

[`file.output`]— In the `file.output` section, the output files for the calculation results can be specified. The items as output for each calculation mode are described in Sec. 3.2.3.

3.2.2. Interaction definition files

H-wave supports a set of interaction definition files that define the Hamiltonian. They are specified in the [`file.input.interaction`] section of the parameter file with keywords and associated file names. These files consist of geometry information (labeled as `Geometry`), transfer integral (labeled as `Trans` for UHFr or `Transfer` for UHFk and RPA), and two-body interaction terms with names based on the convention adopted in other software for quantum lattice models, $\mathcal{H}\Phi$ [46, 47] and mVMC [48], as listed in Table 1. For the RPA calculations, an external field to the one-body interaction term can be introduced using the keyword `Extern`. The form of the term added to the transfer term $T_{\alpha\sigma,\beta\sigma'}(r)$ reads

$$T_{\alpha\sigma,\beta\sigma'}(r) \to T_{\alpha\sigma,\beta\sigma'}(r) + h(\boldsymbol{\sigma}^z)_{\sigma\sigma'} B_{\alpha\beta}(r), \quad (28)$$

where $B_{\alpha\beta}(r)$ is the external field given in the file specified by `Extern` keyword, h is the coefficient specified by `extern_coeff` parameter, and $\boldsymbol{\sigma}^z$ is the z-component of the Pauli matrix.

The file format of the interaction definition files for the UHFr calculations follows the *Expert-mode* format of $\mathcal{H}\Phi$, which is a text-based format with header lines, followed by content in which the indices i and j and the value of the coefficient, for example, J_{ij}, are listed for the interaction term.

Table 1: Keywords for the interaction types and their descriptions are summarized. $c_{i\alpha\uparrow(\downarrow)}^\dagger$ and $c_{i\alpha\uparrow(\downarrow)}$ denote the creation and annihilation operators, respectively, of electrons at site i and orbital α with spin-up (spin-down). $N_{i\alpha\uparrow(\downarrow)} = c_{i\alpha\uparrow(\downarrow)}^\dagger c_{i\alpha\uparrow(\downarrow)}$, and $N_{i\alpha} = N_{i\alpha\uparrow} + N_{i\alpha\downarrow}$. $S_{i\alpha}^\nu = \frac{1}{2}\sum_{\sigma,\sigma'} c_{i\alpha\sigma}^\dagger \sigma_{\sigma\sigma'}^\nu c_{i\alpha\sigma'}$ where $\boldsymbol{\sigma}^k$ is the Pauli matrix, and $\boldsymbol{\sigma}^\pm = \frac{1}{2}(\boldsymbol{\sigma}^x \pm i\boldsymbol{\sigma}^y)$.

Keyword	Description
`Transfer` (or `Trans`)	Transfer term denoted by $T_{i\alpha j\beta} c_{i\alpha\sigma}^\dagger c_{j\beta\sigma}$ (`spin_orbital = False`), or $T_{i(\alpha,\sigma)j(\beta,\sigma')} c_{i(\alpha,\sigma)}^\dagger c_{j(\beta,\sigma')}$ (`spin_orbital = True`)
`InterAll`	A general two-body interaction term of the form $I_{ijkl\sigma_1\sigma_2\sigma_3\sigma_4} c_{i\sigma_1}^\dagger c_{j\sigma_2} c_{k\sigma_3}^\dagger c_{l\sigma_4}$ (only for UHFr),
`CoulombIntra`	On-site Coulomb interaction denoted by $U_{i\alpha} N_{i\alpha\uparrow} N_{i\alpha\downarrow}$
`CoulombInter`	Off-site Coulomb interaction denoted by $V_{i\alpha j\beta} N_{i\alpha} N_{j\beta}$
`Hund`	Hund coupling interaction denoted by $J_{i\alpha j\beta}^{\text{Hund}} (N_{i\alpha\uparrow} N_{j\beta\uparrow} + N_{i\alpha\downarrow} N_{j\beta\downarrow})$
`Ising`	Ising interaction denoted by $J_{i\alpha j\beta}^{\text{Ising}} S_{i\alpha}^z S_{j\beta}^z$
`Exchange`	Exchange interaction denoted by $J_{i\alpha j\beta}^{\text{Ex}} S_{i\alpha}^+ S_{j\beta}^-$
`PairLift`	The interaction denoted by $J_{i\alpha j\beta}^{\text{PairLift}} c_{i\alpha\uparrow}^\dagger c_{i\alpha\downarrow} c_{j\beta\uparrow}^\dagger c_{j\beta\downarrow}$
`PairHop`	The interaction denoted by $J_{i\alpha j\beta}^{\text{PairHop}} c_{i\alpha\uparrow}^\dagger c_{j\beta\uparrow} c_{i\alpha\downarrow}^\dagger c_{j\beta\downarrow}$ (only for UHFr mode)

Further details have been provided in the manuals of $\mathcal{H}\Phi$ [25] and mVMC [23].

For the UHFk and RPA calculations, a WANNIER90-like format [3] is adopted for the interaction definition because translational symmetry is assumed in these methods. In this format, the coefficient of the interaction term $J_{i\alpha j\beta} = J_{\alpha\beta}(r_{ij})$ can be expressed by the components of the three-dimensional translation vector r_{ij}, the orbital indices α and β, and the value in each line. H-wave allows zero components to be omitted. A few examples of the interaction definition files for the UHFk calculations are presented in the following.

The `Transfer` term can be expressed as

`Transfer in Wannier90-like format for uhfk`

```
1
9
 1 1 1 1 1 1 1 1 1
  -1    0    0    1    1  -1.000   0.000
   0   -1    0    1    1  -1.000   0.000
   0    1    0    1    1  -1.000   0.000
   1    0    0    1    1  -1.000   0.000
```

The on-site Coulomb interaction (`CoulombIntra`) can be expressed as

```
CoulombIntra in Wannier90-like format for uhfk
1
1
 1
   0    0    0    1    1   4.000   0.000
```

The geometry definition (`Geometry`) can be expressed as

```
1.000   0.000   0.000
0.000   1.000   0.000
0.000   0.000   1.000
1
     0.000e+00      0.000e+00      0.000e+00
```

The *file specifications* section of the H-wave manual [42] can be referred to for details on the file formats.

Such files can be generated from a simple input using the STDFACE library [44]. An example of the input file (`stan.in`) has been provided

```
model     = "Hubbard"
lattice   = "square"
W         = 4
L         = 4
t         = 1.0
U         = 4.0
calcmode  = "uhfk"
exportall = 0
```

3.2.3. Output

H-wave outputs the calculation results to the files according to the settings specified in the [file.output] section of the input parameter file. A brief overview of the main parameters in [file.output] is discussed.

In real space UHFA calculations, the following keywords can be used.

- energy: The total energy and its components for each interaction term, the number of electrons, and the value of S^z are written to a text file in the `item=value` format.

- eigen: The eigenvalues and eigenvectors are provided as outputs in NUMPY zip files [49]. For a fixed S^z, the spin-up and spin-down components are stored in separate files with `spin-up` or `spin-down` prefix. Otherwise, the eigenvalues and eigenvectors are provided as outputs in a single file with a prefix `sz-free`.

- green: The Green's function is provided as an output in a text file with indices specified in the `OnebodyG` file.

- fij: In real-space UHFA calculations, the coefficients of the pair-product wave functions f_{ij}, which are equivalent to the converged one-body wave functions, are provided as outputs. They are written to a text-format file specified by `fij`. Further details on the relationship between the HFA solutions and the pair-product wave functions have been provided in Ref. [48].

In the `UHFk` calculations, the following keywords can be used.

- energy: The value of the total energy and its components for each interaction term, the number of electrons, and the value of S^z are written to a text file in the `item=value` format. An example output of energy is shown below.

```
Energy_Total       = -12.56655452028271
Energy_Band        = -4.507491115073952
Energy_CoulombIntra = -8.059063405208757
NCond   = 15.999999999999996
Sz      = -7.239267874048494e-08
```

- eigen: The eigenvalues and eigenvectors are provided as outputs in a NUMPY zip file.

- green: The Green's function is provided as an output in a NUMPY zip file.

- rpa: The modified Transfer term representing the approximated one-body Hamiltonian is provided as an output in a NUMPY zip file for an initial value of the RPA calculation.

In the RPA calculations, the following keywords can be used.

- chi0q: The irreducible susceptibility matrix $\chi^{(0)}(\boldsymbol{q}, i\nu_n)$ is provided as an output in a NUMPY zip file.

- chiq: The susceptibility matrix $\chi(\boldsymbol{q}, i\nu_n)$ is provided as an output in a NUMPY zip file.

4. Applications

In this section, three examples of H-wave have been introduced, which include methods to calculate a ground-state phase diagram at zero temperature (zero-temperature UHFk), finite-temperature physical quantities (finite-temperature UHFk), and charge and spin susceptibilities at finite temperatures (RPA). Tutorials on H-wave have been uploaded to a repository [50], which includes several other samples of H-wave and examples presented in this paper.

4.1. Ground state of the extended Hubbard model on a square lattice

As a simple application of the UHFk calculation at zero temperature, the ground states of the extended Hubbard model on a square lattice at half-filling were considered. In the extended Hubbard model, a first-order quantum phase transition is expected from the antiferromagnetic (AF) phase to the charge-ordered (CO) phase by changing the off-site Coulomb interactions. The extended Hubbard model is defined as

$$\mathcal{H} = -t \sum_{\langle i,j \rangle} \sum_{\sigma=\uparrow\downarrow} \left[c_{i\sigma}^\dagger c_{j\sigma} + c_{j\sigma}^\dagger c_{i\sigma} \right] \\ + U \sum_i N_{i\uparrow} N_{i\downarrow} + V \sum_{\langle i,j \rangle} N_i N_j, \quad (29)$$

where $\langle i,j \rangle$ means the nearest neighbor pairs on the square lattice, $N_{i\sigma} = c_{i\sigma}^\dagger c_{i\sigma}$ represents the number operator of the spin σ at the site i, $N_i = N_{i\uparrow} + N_{i\downarrow}$, and U and V denote the onsite and offsite Coulomb repulsion. The hopping constant t was used as the unit of energy. (Hereafter, $t = 1$.) The case of half-filling was considered, in which the number of electrons was taken to be equal to the number of sites. Two phases are expected to appear as the ground states (Fig. 5(a)). For $V/U \lesssim 1/4$, the AF phase where the neighboring spins align in opposite directions to each other emerges. The AF phase is characterized by the staggered magnetization defined as $S(\mathbf{Q}) = \sum_i S_i^z \exp(-i\mathbf{Q} \cdot \mathbf{r}_i)/N_{\mathrm{cell}}$ with $\mathbf{Q} = (\pi, \pi)$, where $S_i^z = (N_{i\uparrow} - N_{i\downarrow})/2$ and the summation runs over sites in the unit cell, and N_{cell} is the number of sites in the unit cell. For $V/U \gtrsim 1/4$, the CO phase becomes the ground state where the doubly occupied sites are arranged in a checkerboard pattern. The CO phase is characterized by the staggered density defined as $N(\mathbf{Q}) = \sum_i (N_{i\uparrow} + N_{i\downarrow}) \exp(-i\mathbf{Q} \cdot \mathbf{r}_i)/N_{\mathrm{cell}}$.
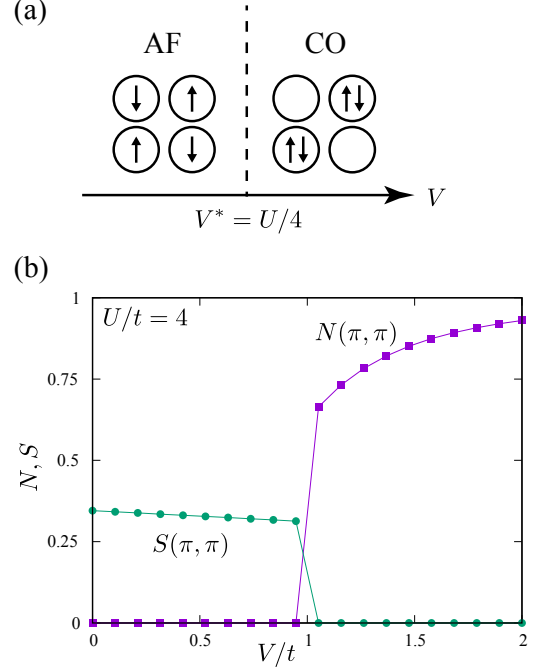

Figure 5: (a) Expected phase diagram of the extended Hubbard model on the square lattice at half-filling in the strong coupling limit. (b) V dependencies of the staggered magnetization $S(\pi, \pi)$ (green circles) and the staggered charge density $N(\pi, \pi)$ (blue squares) of the extended Hubbard model on the square lattice with $U = 4$ at half-filling calculated by the UHFk mode of H-wave. A first-order phase transition between the AF phase and the CO phase occurs around $V/U = 1/4$.

Figure 5 (b) shows the V dependence of $S(\pi, \pi)$ and $N(\pi, \pi)$. As expected, the first-order phase transition between the AF and the CO phases was observed at $V/t = 1 (= U/4t)$. A sample script is available in `samples/UHFk/CDW_SDW` directory of the tutorial repository. By executing the script `run.py`, the results shown in Figure 5 (b) can be reproduced.

4.2. Finite-temperature properties of the Hubbard model on a cubic lattice

H-wave supports finite-temperature mean-field calculations. In this section, a typical simple example involving the estimation of Néel temperature for the Hubbard model on a cubic lattice at half-filling has been discussed. The model was defined as

$$\mathcal{H} = \sum_{\mathbf{r}} \left[-t \sum_{\nu,\sigma} \sum_{\boldsymbol{\delta}=\pm\boldsymbol{a}_\nu} c_{\mathbf{r}\sigma}^\dagger c_{\mathbf{r}+\boldsymbol{\delta},\sigma} + U N_{\mathbf{r}\uparrow} N_{\mathbf{r}\downarrow} \right], \quad (30)$$

10

where $\boldsymbol{a}_\nu$ denotes the translation vector along the α-axis, and $\nu = x, y$, and z.

Figure 6(a) shows the dependency of magnetization on temperature for the Hubbard model on a cubic lattice at half-filling. The magnetization presented along the z axis was defined as

$$m_z = \frac{1}{2N_{\text{site}}} \sum_{\boldsymbol{r}} |\langle n_{\boldsymbol{r}\uparrow} - n_{\boldsymbol{r}\downarrow} \rangle|. \tag{31}$$

The number of sites N_{site} was denoted as $N_{\text{site}} = L^3$, where L denotes the linear dimensions of a cubic structure. The magnetization was observed to be finite at the critical temperature $T_{\text{Néel}}$. For this study, $T_{\text{Néel}}$ was regarded as the lowest temperature at which m_z had a value lesser than 10^{-4}.

Figure 6 (b) shows the interaction dependence of Néel temperature $T_{\text{Néel}}$. The results suggested that $T_{\text{Néel}}$ monotonically increased with the interaction U/t. However, this tendency was a well-known artifact of the HFA. For a strong-coupling limit, $T_{\text{Néel}}$ is expected to decrease with increase in U/t [51–53] because it is governed by super-exchange interactions $J = 4t^2/U$. To correctly reproduce such a tendency, many-body correlations beyond the HFA must necessarily be included.

4.3. Charge and spin susceptibilities of the extended Hubbard model on a square lattice

In this sub-section, charge and spin susceptibilities of the extended Hubbard model on a square lattice defined in Eq. (29) using the RPA are discussed. In order to reproduce the numerical results shown in Fig. 1 of Ref. [54], the electron filling was set as $3/4$ and $T = 0.01$. The cell size was set to $L_x = L_y = 128$. Sample files and scripts were used from the `samples/RPA/kobayashi_2004` directory of the tutorial repository.

Figure 7 shows spin and charge susceptibilities $\chi_s(\boldsymbol{q}, 0)$, $\chi_c(\boldsymbol{q}, 0)$ at $(U, V) = (3.7, 0)$ and $(0, 0.8)$, respectively, where $\chi_s(\boldsymbol{q}, 0)$ and $\chi_c(\boldsymbol{q}, 0)$ are defined as $1/2 \sum_{\sigma\sigma'} \sigma\sigma' \chi_{\sigma\sigma'}(\boldsymbol{q}, 0)$ with $\sigma = +(-)$ for $\uparrow (\downarrow)$ and $1/2 \sum_{\sigma\sigma'} \chi_{\sigma\sigma'}(\boldsymbol{q}, 0)$, respectively. At $(U, V) = (3.7, 0)$, $\chi_s(\boldsymbol{q}, 0)$ showed a sharp peak around $\boldsymbol{Q}_{\text{nest}} = (\pi, \pi/2)$ due to the nesting condition as shown in the inset of Fig. 7. This peak developed with increasing U and diverged when the spin-density-wave transition occurred. At $(U, V) = (0, 0.8)$, $\chi_c(\boldsymbol{q}, 0)$ exhibited sharp peaks around $(\pi, \pi/2)$ and $(\pi/2, \pi/2)$. The first peak originated from the nesting condition, whereas the second peak originated from the anisotropy of $V_{\boldsymbol{q}}$,
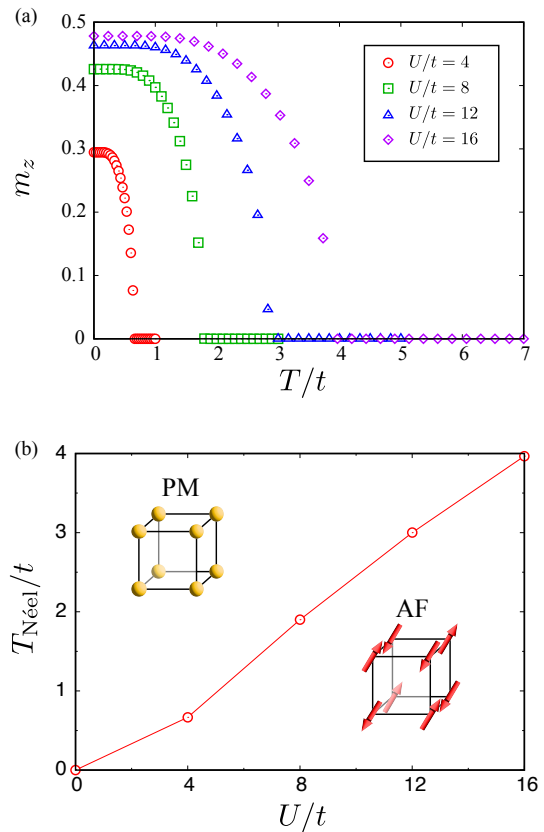

Figure 6: Magnetic properties of the Hubbard model on the cubic lattice at half-filling for $L = 12$. (a) Temperature dependence of the magnetic moment along the z-axis. Red circles, green squares, blue triangles, and purple diamonds denote the mean-field results for $U/t = 4$, 8, 12, and 16, respectively. (b) Interaction dependence of the Néel temperature $T_{\text{Néel}}$. Red circles denote the mean-field results. Insets represent schematics of paramagnetic (PM) and antiferromagnetic (AF) states.

which had a negative peak at (π, π), in addition to the nesting conditions. The latter peak developed with an increase in V and diverged when a charge-density wave (or charge ordering) transition occurred. The obtained results aligned with those shown in Fig. 1 of Ref. [54].

5. Summary

In this paper, we introduced H-wave, which can perform the unrestricted Hartree–Fock approximation (UHFA) and the random phase approximation (RPA). UHFA and RPA in wave-number space enable numerical analyses of electron correlation effects in periodic electron systems within fluctuations up to the first order at a low computational
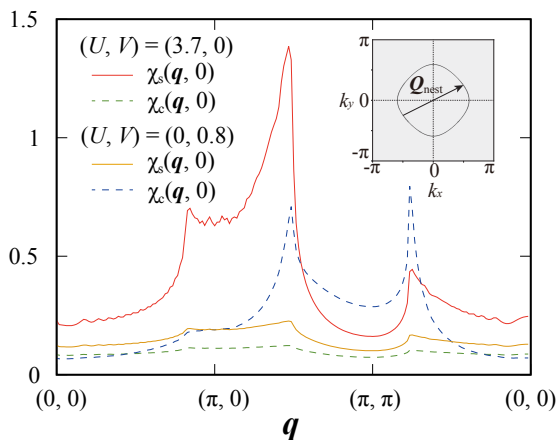
Figure 7: Spin and charge susceptibilities of the extended Hubbard model at $T = 0.01$. The interaction parameters are set as $(U, V) = (3.7, 0)$ and $(0, 0.8)$, respectively. The inset shows the Fermi surface (solid line) and the nesting vector $\boldsymbol{Q}_{\mathrm{nest}} \equiv (\pi, \pi/2)$.

cost. H-wave is open-source software with simple and flexible user interface. Users can execute UHFA and RPA for widely studied quantum lattice models such as the Hubbard model by preparing only one input file with less than ten lines. Furthermore, the input files of one- and two-body interactions describing effective models can be imported from first principles calculations using the WANNIER90 format such as RESPACK. This enables a high-throughput connection between the first principles calculations and H-wave. The resulting files can be used as input files for softwares that handle strong correlation effects, such as mVMC [48]. H-wave is included in MateriApps LIVE! [55, 56], an environment for computational materials science, and MateriApps Installer [56, 57], a collection of scripts for installing materials science calculation software. These provide the environment to easy application of H-wave.

In the future, we plan to develop the following functions based on the experience gained from our previous works; (a) function to calculate the quantities corresponding to the experimentally measured dynamic susceptibilities, such as magnetic susceptibility and spin-lattice relaxation rate for nuclear magnetic resonance and conductivity [58–61], (b) function to solve the linear Eliashberg equation evaluating the superconducting transition temperature and order parameters by considering pairing interactions mediated by charge and spin fluctua-

tions [26, 29, 54, 62], and (c) function to treat approximations beyond RPA such as fluctuation exchange approximation (FLEX) and vertex corrections [63–67].

Acknowledgments

References

[1] M. Imada, A. Fujimori, Y. Tokura, Metal-insulator transitions, Rev. Mod. Phys. 70 (1998) 1039–1263. doi:10.1103/RevModPhys.70.1039.
URL https://link.aps.org/doi/10.1103/RevModPhys.70.1039

[2] P. Fazekas (Ed.), Lecture Notes on Electron Correlation and Magnetism (Series in Modern Condensed Matter Physics), World Scientific, 1999. doi:10.1142/2945.
URL https://www.worldscientific.com/doi/abs/10.1142/2945

[3] G. Pizzi, V. Vitale, R. Arita, S. Blügel, F. Freimuth, G. Géranton, M. Gibertini, D. Gresch, C. Johnson, T. Koretsune, J. Ibañez-Azpiroz, H. Lee, J.-M. Lihm, D. Marchand, A. Marrazzo, Y. Mokrousov, J. I. Mustafa, Y. Nohara, Y. Nomura, L. Paulatto, S. Poncé, T. Ponweiser, J. Qiao, F. Thöle, S. S. Tsirkin, M. Wierzbowska, N. Marzari, D. Vanderbilt, I. Souza, A. A. Mostofi, J. R. Yates, Wannier90 as a community code: new features and applications, J. Phys. Condens. Matter 32 (2020) 165902. doi:10.1088/1361-648X/ab51ff.
URL https://dx.doi.org/10.1088/1361-648X/ab51ff

[4] F. Aryasetiawan, M. Imada, A. Georges, G. Kotliar, S. Biermann, A. I. Lichtenstein, Frequency-dependent local interactions and low-energy effective models from electronic structure calculations, Phys. Rev. B 70 (2004) 195104. doi:10.1103/PhysRevB.70.195104.
URL https://link.aps.org/doi/10.1103/PhysRevB.70.195104

[5] M. Imada, T. Miyake, Electronic structure calculation by first principles for strongly correlated electron systems, Journal of the Physical Society of Japan 79 (11) (2010) 112001. arXiv:https://doi.org/10.1143/JPSJ.79.112001, doi:10.1143/JPSJ.79.112001.
URL https://doi.org/10.1143/JPSJ.79.112001

[6] E. Dagotto, Correlated electrons in high-temperature superconductors, Rev. Mod. Phys. 66 (1994) 763–840. doi:10.1103/RevModPhys.66.763.
URL https://link.aps.org/doi/10.1103/RevModPhys.66.763

[7] J. Gubernatis, N. Kawashima, P. Werner (Eds.), Quantum Monte Carlo Methods, Cambridge University Press, 2016. doi:10.1017/CBO9780511902581.

[8] U. Schollwöck, The density-matrix renormalization group, Rev. Mod. Phys. 77 (2005) 259–315. doi:10.1103/RevModPhys.77.259.
URL https://link.aps.org/doi/10.1103/RevModPhys.77.259

[9] Román Orús, A practical introduction to tensor networks: Matrix product states and projected entangled pair states, Ann. Phys. 349 (2014) 117–158. doi:10.1016/j.aop.2014.06.013.
URL https://www.sciencedirect.com/science/article/pii/S0003491614001596

[10] R. Orús, Tensor networks for complex quantum systems, Nature Reviews Physics 1 (9) (2019) 538–550. doi:10.1038/s42254-019-0086-7.

[11] H. Fehske, R. Schneider, Weiße (Eds.), Computational Many-Particle Physics, Springer, 2008. doi:10.1007/978-3-540-74686-7.

[12] A. Avella, F. Mancini (Eds.), Strongly Correlated Systems, Springer Berlin Heidelberg, 2013. doi:10.1007/978-3-642-35106-8.
URL https://doi.org/10.1007/978-3-642-35106-8

[13] G. D. Mahan (Ed.), Many-Particle Physics, 3rd Edition, Springer, 2000. doi:10.1007/978-1-4757-5714-9.

[14] P. Ring, P. Schuck, The nuclear many-body problem, Springer Berlin, Heidelberg, 1980.

[15] J. E. Hirsch, Two-dimensional Hubbard model: Numerical simulation study, Phys. Rev. B 31 (1985) 4403–4419. doi:10.1103/PhysRevB.31.4403.
URL https://link.aps.org/doi/10.1103/PhysRevB.31.4403

[16] D. R. Penn, Stability theory of the magnetic phases for a simple model of the transition metals, Phys. Rev. 142 (1966) 350–365. doi:10.1103/PhysRev.142.350.
URL https://link.aps.org/doi/10.1103/PhysRev.142.350

[17] T. Mizokawa, A. Fujimori, Electronic structure and orbital ordering in perovskite-type 3d transition-metal oxides studied by Hartree-Fock band-structure calculations, Phys. Rev. B 54 (1996) 5368–5380. doi:10.1103/PhysRevB.54.5368.
URL https://link.aps.org/doi/10.1103/PhysRevB.54.5368

[18] H. Seo, C. Hotta, H. Fukuyama, Toward Systematic Understanding of Diversity of Electronic Properties in Low-Dimensional Molecular Solids, Chem. Rev. 104 (2004) 5005–5036, pMID: 15535640. doi:10.1021/cr030646k.
URL https://doi.org/10.1021/cr030646k

[19] A. L. Fetter, J. D. Walecka, Quantum Theory of Many-Particle Systems, McGraw-Hill, Boston, 1971.

[20] L. P. Kadanoff, G. Baym (Eds.), Quantum Statistical Mechanics: Green's Function Methods in Equilibrium and Nonequilibrium Problems, Westview Press, 1994.

[21] TRIQS (Toolbox for Research on Interacting Quantum Systems), https://triqs.github.io/triqs/latest/.

[22] O. Parcollet, M. Ferrero, T. Ayral, H. Hafermann, I. Krivenko, L. Messio, P. Seth, Triqs: A toolbox for research on interacting quantum systems, Comput. Phys. Commun. 196 (2015) 398 – 415. doi:http://dx.doi.org/10.1016/j.cpc.2015.04.023.

[23] https://issp-center-dev.github.io/mVMC/doc/master/en/index.html.

[24] H-wave: a Python package for performing unrestricted Hartree-Fock calculations and random phase approximation calculations for itinerant electron systems,
https://www.pasums.issp.u-tokyo.ac.jp/h-wave/en.

[25] https://issp-center-dev.github.io/HPhi/manual/master/en/html/index.html.

[26] A. Kobayashi, S. Katayama, K. Noguchi, Y. Suzumura, Superconductivity in Charge Ordered Organic Conductor —α-$(ET)_2I_3$ Salt—, Journal of the Physical Society of Japan 73 (11) (2004) 3135–3148. doi:10.1143/JPSJ.73.3135.
URL https://doi.org/10.1143/JPSJ.73.3135

[27] T. Takimoto, T. Hotta, K. Ueda, Strong-coupling theory of superconductivity in a degenerate Hubbard model, Phys. Rev. B 69 (2004) 104504. doi:10.1103/PhysRevB.69.104504.
URL https://link.aps.org/doi/10.1103/PhysRevB.69.104504

[28] K. Kubo, T. Hotta, Orbital-controlled superconductivity in f-electron systems, Journal of the Physical Society of Japan 75 (8) (2006) 083702. arXiv:https://doi.org/10.1143/JPSJ.75.083702, doi:10.1143/JPSJ.75.083702.
URL https://doi.org/10.1143/JPSJ.75.083702

[29] K. Yoshimi, M. Nakamura, H. Mori, Superconductivity in the vicinity of charge ordered state in organic conductor β-($meso$-DMBEDT-TTF)$_2$PF$_6$, Journal of the Physical Society of Japan 76 (2) (2007) 024706. arXiv:https://doi.org/10.1143/JPSJ.76.024706, doi:10.1143/JPSJ.76.024706.
URL https://doi.org/10.1143/JPSJ.76.024706

[30] A. Kobayashi, Y. Suzumura, M. Higa, R. Kondo, S. Kagoshima, H. Nishikawa, Charge ordered metal and pressure-induced superconductivity in the two-dimensional organic conductor β''-(DODHT)$_2$PF$_6$, Journal of Physics: Condensed Matter 20 (12) (2008) 125205. doi:10.1088/0953-8984/20/12/125205.
URL https://dx.doi.org/10.1088/0953-8984/20/12/125205

[31] S. Graser, T. A. Maier, P. J. Hirschfeld, D. J. Scalapino, Near-degeneracy of several pairing channels in multi-orbital models for the Fe pnictides, New Journal of Physics 11 (2) (2009) 025016. doi:10.1088/1367-2630/11/2/025016.
URL https://dx.doi.org/10.1088/1367-2630/11/2/025016

[32] H. Kontani, T. Saito, S. Onari, Origin of orthorhombic transition, magnetic transition, and shear-modulus softening in iron pnictide superconductors: Analysis based on the orbital fluctuations theory, Phys. Rev. B 84 (2011) 024528. doi:10.1103/PhysRevB.84.024528.
URL https://link.aps.org/doi/10.1103/PhysRevB.84.024528

[33] M. Altmeyer, D. Guterding, P. J. Hirschfeld, T. A. Maier, R. Valentí, D. J. Scalapino, Role of vertex corrections in the matrix formulation of the random phase approximation for the multiorbital Hubbard model, Phys. Rev. B 94 (2016) 214515. doi:10.1103/PhysRevB.94.214515.
URL https://link.aps.org/doi/10.1103/PhysRevB.94.214515

[34] C. R. Harris, K. J. Millman, S. J. van der Walt, R. Gommers, P. Virtanen, D. Cournapeau, E. Wieser, J. Taylor, S. Berg, N. J. Smith, R. Kern, M. Picus, S. Hoyer, M. H. van Kerkwijk, M. Brett, A. Haldane, J. F. del Río, M. Wiebe, P. Peterson, P. Gérard-Marchant, K. Sheppard, T. Reddy, W. Weckesser, H. Abbasi, C. Gohlke, T. E. Oliphant, Array programming with

13

NumPy, Nature 585 (7825) (2020) 357–362. doi:10.
1038/s41586-020-2649-2.
URL https://doi.org/10.1038/s41586-020-2649-2

[35] https://numpy.org/.

[36] P. Virtanen, R. Gommers, T. E. Oliphant, M. Haber-
land, T. Reddy, D. Cournapeau, E. Burovski, P. Pe-
terson, W. Weckesser, J. Bright, S. J. van der Walt,
M. Brett, J. Wilson, K. J. Millman, N. Mayorov,
A. R. J. Nelson, E. Jones, R. Kern, E. Larson, C. J.
Carey, İ. Polat, Y. Feng, E. W. Moore, J. Vander-
Plas, D. Laxalde, J. Perktold, R. Cimrman, I. Hen-
riksen, E. A. Quintero, C. R. Harris, A. M. Archibald,
A. H. Ribeiro, F. Pedregosa, P. van Mulbregt, SciPy
1.0 Contributors, SciPy 1.0: Fundamental Algorithms
for Scientific Computing in Python, Nature Methods 17
(2020) 261–272. doi:10.1038/s41592-019-0686-2.

[37] https://scipy.org/.

[38] https://github.com/hukkin/tomli.

[39] https://requests.readthedocs.io/en/latest/.

[40] https://pypi.org/.

[41] https://github.com/issp-center-dev/H-wave.

[42] https://issp-center-dev.github.io/H-wave/
manual/main/en/html/index.html.

[43] K. Nakamura, Y. Yoshimoto, Y. Nomura, T. Tadano,
M. Kawamura, T. Kosugi, K. Yoshimi, T. Mis-
awa, Y. Motoyama, Respack: An ab initio tool for
derivation of effective low-energy model of mate-
rial, Comput. Phys. Commun. 261 (2021) 107781.
doi:https://doi.org/10.1016/j.cpc.2020.107781.
URL https://www.sciencedirect.com/science/
article/pii/S001046552030391X

[44] https://github.com/issp-center-dev/StdFace.

[45] https://toml.io/.

[46] M. Kawamura, K. Yoshimi, T. Misawa, Y. Yamaji,
S. Todo, N. Kawashima, Quantum lattice model solver
$\mathcal{H}\Phi$, Computer Physics Communications 217 (2017)
180–192. doi:10.1016/j.cpc.2017.04.006.
URL https://www.sciencedirect.com/science/
article/pii/S0010465517301200

[47] K. Ido, M. Kawamura, Y. Motoyama, K. Yoshimi,
Y. Yamaji, S. Todo, N. Kawashima, T. Misawa, Up-
date of $\mathcal{H}\Phi$: Newly added functions and methods in
versions 2 and 3 (2023). arXiv:2307.13222.

[48] T. Misawa, S. Morita, K. Yoshimi, M. Kawamura,
Y. Motoyama, K. Ido, T. Ohgoe, M. Imada, T. Kato,
mVMC—Open-source software for many-variable vari-
ational Monte Carlo method, Comput. Phys. Commun.
235 (2019) 447–462. doi:10.1016/j.cpc.2018.08.014.
URL https://www.sciencedirect.com/science/
article/pii/S0010465518303102

[49] https://numpy.org/devdocs/reference/generated/
numpy.lib.format.html.

[50] https://isspns-gitlab.issp.u-tokyo.ac.jp/
hwave-dev/hwave-gallery.

[51] Y. Kakehashi, H. Hasegawa, Magnetic phase diagram
of the half-filled Hubbard model for a simple cubic lat-
tice, Phys. Rev. B 36 (1987) 4066–4069. doi:10.1103/
PhysRevB.36.4066.
URL https://link.aps.org/doi/10.1103/PhysRevB.
36.4066

[52] G. Rohringer, A. Toschi, A. Katanin, K. Held, Critical
properties of the half-filled Hubbard model in three
dimensions, Phys. Rev. Lett. 107 (2011) 256402.
doi:10.1103/PhysRevLett.107.256402.
URL https://link.aps.org/doi/10.1103/

PhysRevLett.107.256402

[53] A. Mukherjee, N. D. Patel, S. Dong, S. Johnston,
A. Moreo, E. Dagotto, Testing the Monte Carlo–
mean field approximation in the one-band Hubbard
model, Phys. Rev. B 90 (2014) 205133. doi:10.1103/
PhysRevB.90.205133.
URL https://link.aps.org/doi/10.1103/PhysRevB.
90.205133

[54] A. Kobayashi, Y. Tanaka, M. Ogata, Y. Suzu-
mura, Charge-Fluctuation-Induced Superconducting
State in Two-Dimensional Quarter-Filled Electron Sys-
tems, Journal of the Physical Society of Japan 73 (5)
(2004) 1115–1118. doi:10.1143/JPSJ.73.1115.
URL https://doi.org/10.1143/JPSJ.73.1115

[55] MateriApps LIVE!: an environment for compu-
tational materials science., http://cmsi.github.io/
MateriAppsLive/.

[56] Y. Motoyama, K. Yoshimi, T. Kato, S. Todo,
MateriApps LIVE! and MateriApps Installer: En-
vironment for starting and scaling up materials
science simulations, SoftwareX 20 (2022) 101210.
doi:10.1016/j.softx.2022.101210.
URL https://www.sciencedirect.com/science/
article/pii/S2352711022001285

[57] MateriApps Installer: a script collection for installation
of computational materials science programs., https:
//github.com/wistaria/MateriAppsInstaller.

[58] R. Kubo, Statistical-mechanical theory of irreversible
processes. I. General theory and simple applications
to magnetic and conduction problems, Journal of
the Physical Society of Japan 12 (6) (1957) 570–
586. arXiv:https://doi.org/10.1143/JPSJ.12.570,
doi:10.1143/JPSJ.12.570.
URL https://doi.org/10.1143/JPSJ.12.570

[59] T. Moriya, The effect of electron-electron interaction
on the nuclear spin relaxation in metals, Journal of
the Physical Society of Japan 18 (4) (1963) 516–
520. arXiv:https://doi.org/10.1143/JPSJ.18.516,
doi:10.1143/JPSJ.18.516.
URL https://doi.org/10.1143/JPSJ.18.516

[60] T. Imai, Analysis of nuclear relaxation experiments in
high T_c oxides based on Mila-Rice Hamiltonian, Journal
of the Physical Society of Japan 59 (7) (1990) 2508–
2521. arXiv:https://doi.org/10.1143/JPSJ.59.2508,
doi:10.1143/JPSJ.59.2508.
URL https://doi.org/10.1143/JPSJ.59.2508

[61] D. Ohki, K. Yoshimi, A. Kobayashi, Interaction-
induced quantum spin Hall insulator in the organic
Dirac electron system α-(BEDT-TSeF)$_2$I$_3$, Phys. Rev.
B 105 (2022) 205123. doi:10.1103/PhysRevB.105.
205123.
URL https://link.aps.org/doi/10.1103/PhysRevB.
105.205123

[62] H. J. Vidberg, J. W. Serene, Solving the Eliashberg
equations by means of N-point Padé approximants,
Journal of Low Temperature Physics 29 (3) (1977) 179–
192. doi:10.1007/BF00655090.
URL https://doi.org/10.1007/BF00655090

[63] N. Bickers, D. Scalapino, Conserving approxima-
tions for strongly fluctuating electron systems.
I. Formalism and calculational approach, Annals
of Physics 193 (1) (1989) 206–251. doi:https:
//doi.org/10.1016/0003-4916(89)90359-X.
URL https://www.sciencedirect.com/science/
article/pii/000349168990359X

[64] N. E. Bickers, D. J. Scalapino, S. R. White, Conserving approximations for strongly correlated electron systems: Bethe-Salpeter equation and dynamics for the two-dimensional Hubbard model, Phys. Rev. Lett. 62 (1989) 961–964. doi:10.1103/PhysRevLett.62.961.
URL https://link.aps.org/doi/10.1103/PhysRevLett.62.961

[65] K. Yoshimi, T. Kato, H. Maebashi, Enhanced spin susceptibility toward the charge-ordering transition in a two-dimensional extended Hubbard model, Journal of the Physical Society of Japan 78 (10) (2009) 104002. arXiv:https://doi.org/10.1143/JPSJ.78.104002, doi:10.1143/JPSJ.78.104002.
URL https://doi.org/10.1143/JPSJ.78.104002

[66] K. Yoshimi, T. Kato, H. Maebashi, Fermi surface deformation near charge-ordering transition, Journal of the Physical Society of Japan 80 (12) (2011) 123707. arXiv:https://doi.org/10.1143/JPSJ.80.123707, doi:10.1143/JPSJ.80.123707.
URL https://doi.org/10.1143/JPSJ.80.123707

[67] K. Yoshimi, H. Maebashi, Coulomb frustrated phase separation in quasi-two-dimensional organic conductors on the verge of charge ordering, Journal of the Physical Society of Japan 81 (6) (2012) 063003. arXiv:https://doi.org/10.1143/JPSJ.81.063003, doi:10.1143/JPSJ.81.063003.
URL https://doi.org/10.1143/JPSJ.81.063003